HHS Public Access

Author manuscript

ACS Appl Mater Interfaces. Author manuscript; available in PMC 2024 July 12.

Published in final edited form as:

ACS Appl Mater Interfaces. 2023 July 12; 15(27): 32121–32135. doi:10.1021/acsami.3c03059.

Nanoscale β-TCP-Laden GelMA/PCL Composite Membrane for Guided Bone Regeneration

Abdel H. Mahmoud,
Department of Cariology, Restorative Sciences, and Endodontics, School of Dentistry, University of Michigan, Ann Arbor, Michigan 48109, United States

Yuanyuan Han,
Department of Cariology, Restorative Sciences, and Endodontics, School of Dentistry, University of Michigan, Ann Arbor, Michigan 48109, United States; Applied Oral Sciences and Community Dental Care, Faculty of Dentistry, The University of Hong Kong, 999077 Hong Kong, China

Renan Dal-Fabbro,
Department of Cariology, Restorative Sciences, and Endodontics, School of Dentistry, University of Michigan, Ann Arbor, Michigan 48109, United States

Arwa Daghrery,
Department of Cariology, Restorative Sciences, and Endodontics, School of Dentistry, University of Michigan, Ann Arbor, Michigan 48109, United States; Department of Restorative Dental Sciences, School of Dentistry, Jazan University, Jazan 45142, Kingdom of Saudi Arabia

Jinping Xu,
Department of Cariology, Restorative Sciences, and Endodontics, School of Dentistry, University of Michigan, Ann Arbor, Michigan 48109, United States

Darnell Kaigler,
Department of Periodontics and Oral Medicine, School of Dentistry and Department of Biomedical Engineering, College of Engineering, University of Michigan, Ann Arbor, Michigan 48109, United States

Sarit B. Bhaduri,
Department of Mechanical, Industrial and Manufacturing Engineering, University of Toledo, Toledo, Ohio 43606-3390, United States; EEC Division, Directorate of Engineering, The National Science Foundation, Alexandria, Virginia 22314, United States

Jos Malda,

Corresponding Author: **Marco C. Bottino** – *Department of Cariology, Restorative Sciences, and Endodontics, School of Dentistry and Department of Biomedical Engineering, College of Engineering, University of Michigan, Ann Arbor, Michigan 48109, United States*; mbottino@umich.edu; Fax: +1-734.936.1597.

Author Contributions

A.H.M., Y.H., and R.D.-F. contributed equally as first authors of this article.

The authors declare no competing financial interest.

ASSOCIATED CONTENT

Supporting Information

The Supporting Information is available free of charge at https://pubs.acs.org/doi/10.1021/acsami.3c03059.

Exemplary SEM images of methacrylated gelatin (GelMA, 150 mg/mL) electrospun fibers following the proposed crosslinking protocol (i.e., 85% isopropyl alcohol immersion plus light-emitting diode [LED] light exposure) (PDF)

Regenerative Medicine Center Utrecht, 3584 CT Utrecht, The Netherlands; Department of Clinical Sciences, Faculty of Veterinary Medicine, Utrecht University, 3508 TC Utrecht, the Netherlands; Department of Orthopedics, University Medical Center Utrecht, 3584 CX Ut Utrecht, The Netherlands

Marco C. Bottino

Department of Cariology, Restorative Sciences, and Endodontics, School of Dentistry and Department of Biomedical Engineering, College of Engineering, University of Michigan, Ann Arbor, Michigan 48109, United States

Abstract

Major advances in the field of periodontal tissue engineering have favored the fabrication of biodegradable membranes with tunable physical and biological properties for guided bone regeneration (GBR). Herein, we engineered innovative nanoscale beta-tricalcium phosphate (β-TCP)-laden gelatin methacryloyl/polycaprolactone (GelMA/PCL-TCP) photocrosslinkable composite fibrous membranes via electrospinning. Chemo-morphological findings showed that the composite microfibers had a uniform porous network and β-TCP particles successfully integrated within the fibers. Compared with pure PCL and GelMA/PCL, GelMA/PCL-TCP membranes led to increased cell attachment, proliferation, mineralization, and osteogenic gene expression in alveolar bone-derived mesenchymal stem cells (aBMSCs). Moreover, our GelMA/PCL-TCP membrane was able to promote robust bone regeneration in rat calvarial critical-size defects, showing remarkable osteogenesis compared to PCL and GelMA/PCL groups. Altogether, the GelMA/PCL-TCP composite fibrous membrane promoted osteogenic differentiation of aBMSCs in vitro and pronounced bone formation in vivo. Our data confirmed that the electrospun GelMA/PCL-TCP composite has a strong potential as a promising membrane for guided bone regeneration.

Graphical Abstract

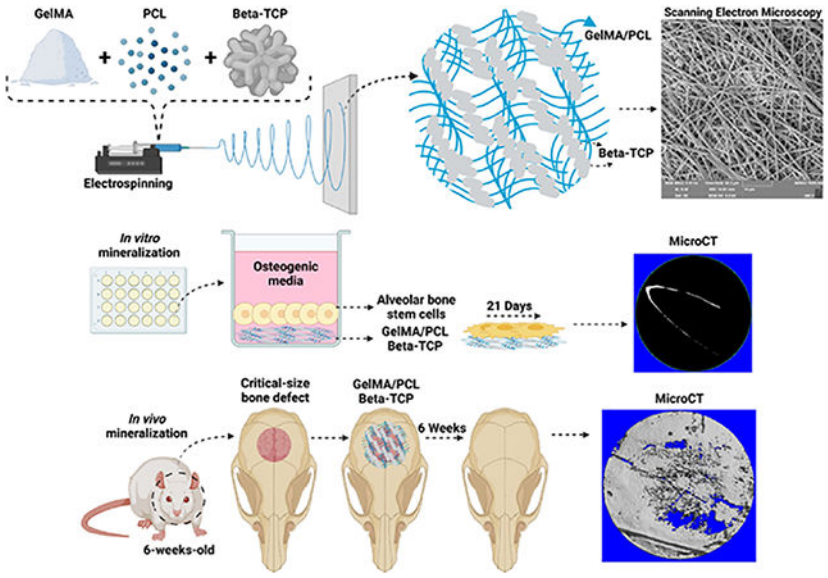

Keywords

bone; regeneration; tissue engineering; electrospinning; extracellular matrix; gelatin

INTRODUCTION

The periodontium is a complex structure consisting of numerous tissues, including cementum, periodontal ligament (PDL), alveolar bone, and the dentogingival junction, with this composite structure providing the anchorage of teeth to the alveolar bone and enabling the dentition to withstand the high loads of masticatory forces.[1] However, the presence of dysbiotic microbial communities in the mouth and the ensuing immune response make the periodontium susceptible to inflammatory disorders, i.e., periodontitis, that irreversibly and progressively destroy the soft and hard tissues of the periodontal complex.[2] This highly prevalent inflammatory disease affects 42% of US adults aged 30 years, with 7.8% presenting with severe periodontitis, which, left untreated, leads to alveolar bone loss, cemental necrosis, and deep periodontal pockets into which additional periodontal pathogens can reside, resulting in tooth loss.[3,4]

Various treatment approaches have been developed in the last two decades to control disease progression, repair periodontal breakdown, and regenerate the periodontium. These treatment modalities include scaling and root planning,[5] open flap debridement,[6,7] autogenous bone grafting,[8] and implantation of biomaterials.[9] Noteworthy, guided bone regeneration (GBR) and guided tissue regeneration (GTR) are the most widely used successful surgical methods to restore lost tooth-supporting structures. GBR and GTR are based on the principles of utilizing a cell occlusive membrane to contain and protect the defect,[10] enabling undisturbed soft (PDL) and hard tissue (bone, cementum) regeneration while also functioning as a barrier to inhibit fibrous tissue ingrowth into the regenerating site.[11–16]

Among the many methods available for membrane production, electrospinning stands out as a simple fabrication process allowing precise control of operating conditions and polymer solution properties.[17] The electrostatic forces produce thin fibers at a nanometer to micrometer scale from pure polymer solutions or additive-modified with inorganic particles (calcium phosphates) or biomolecules (growth factors) to achieve desired biological properties.[18] One of the most broadly used polymers is polycaprolactone (PCL), a slow-degrading semi-crystalline aliphatic polyester with superior compatibility and mechanical characteristics compared to other polyesters.[19,20] Nevertheless, PCL has a hydrophobic character and prolonged degradation rates compared to natural polymers (gelatin), which may impair cell adherence and limit its applications when rapid (3–6 months) degradation is needed.[21–23]

Contrasting to PCL regarding degradability, gelatin methacryloyl (GelMA) is a widely used semi-synthetic biomaterial obtained through the modification of amine-containing side groups of naturally derived gelatin, a denatured product of collagen, with methacrylamide and methacrylate groups.[24] Being derived from a natural source, GelMA facilitates biological interaction between cells and the scaffold and has matrix metalloproteinase

sensitivity, facilitating degradation. However, it presents poor mechanical rigidity and the degradation described above is uncontrollable, making it unsuitable to be utilized alone in periodontal and critical-sized bone defects.[24] Thus, incorporating biologically active ceramic additives, such as bioglasses and calcium phosphates (e.g., hydroxyapatite, HA), is a commonly used method to circumvent the lack of bioactivity and mineralization activity for GBR membranes made from polyester-based materials, such as PCL.[25] However, previous studies reported the fabrication of biomaterials comprising single polymers (PCL) with beta-tricalcium phosphate (beta-TCP) to favor regenerative properties.[26–29] Noteworthily, beta-TCP ($Ca_3(PO_4)_2$), an osteoconductive, osteoinductive, and cell-mediated resorbed synthetic bone graft substitute, is acknowledged to elicit excellent tissue response.[30] However, combining various polymers and ceramics to synergize and optimize their desirable and unique characteristics, such as mechanical and biocompatible features, to achieve bone regeneration still needs to be improved.

Taking advantage of the acceptable mechanical properties of PCL and the ability to adjust its degradation rate by blending with other polymers, we combined it with GelMA with incorporated beta-TCP nanoparticles to improve both the bioactivity and biocompatibility of the composite. Moreover, the degradability was enhanced by the incorporation of the GelMA with further release of TCP particles, which have a shorter degradation time than PCL and also provide Ca^{2+} and PO_4^{3-} ions for bone regeneration locally. These materials were then electrospun to fabricate GelMA/PCL-TCP composite membranes for GBR. Furthermore, structural, mechanical, chemical, in vitro, and in vivo biological properties were systematically evaluated. Specifically, the mechanical integrity of the membranes was investigated under uniaxial tensile loading, while the bone-forming capacity was determined in vitro over 3 weeks. Last, the ability of as-fabricated membranes to promote bone regeneration was determined in an in vivo critical-size calvarial defect rat model over 6 weeks.

RESULTS AND DISCUSSION

The prime objective in periodontal regeneration is to create bioactive constructs with suitable mechanical, physical, and bioactive characteristics to withstand prolonged physical stresses and encourage new tissue formation.[31] While GelMA, a naturally derived material, has bioactive sites for cell binding, PCL has desirable mechanical properties that make it a suitable candidate for reinforcing relatively weaker materials.[27] Although manufacturing composite membranes seem straightforward, fine-tuning their compositional properties is challenging. The integrated properties of the resulting composite membranes pave a new way to solve a key issue when these materials are utilized indivisibly, and their properties are tuned to make biomimetic materials for periodontal tissue engineering. Taken together, our findings demonstrated that the GelMA/PCL-TCP composite membrane had sufficient mechanical properties, improved degradation profile, and biocompatibility, which successfully improved bone regeneration.

Morphological, Chemical, and Thermal Characteristics of TCP Membranes.

The morphological and chemical characteristics of beta-TCP were systematically evaluated using SEM/EDS, FTIR, and XRD. Representative SEM images of the processed membranes are shown in Figure 1A. Bead-free fibrous membranes were obtained with uniform fiber diameters. The means fibers' diameters of synthesized uncrosslinked electrospun fibers were 0.223, 0.243, 0.397, and 0.641 μm for GelMA/PCL, GelMA/PCL-TCP, GelMA, and GelMA-TCP, respectively. The observed higher diameter of GelMA-incorporated TCP (GelMA-TCP), as compared to PCL-incorporated groups, could be correlated with potential variations in the conductivity and viscosity of the solutions[32] that were not examined in this investigation. Importantly, it has been noted that as viscosity increases, chain entanglement increases and fiber diameter increases. On the other hand, increasing the number of charges, as is the case for the PCL-containing solutions, results in a significant stretching of the polymer jet and raises the conductivity of a solution. Hence, it reduces the overall processed fiber's diameter.

Notably, the crosslinked fibers significantly increased in diameter compared to their uncrosslinked counterparts ($p < 0.05$). The fiber diameter was found to be 0.463, 0.433, 1.539, and 2.698 μm for GelMA/PCL, GelMA/PCL-TCP, GelMA, and GelMA-TCP, respectively Figure 1B. Similar to uncrosslinked fiber, solution viscosity and conductivity both contribute to the fiber's diameter, while, as expected, the crosslinking process has the highest impact on the GelMA fiber diameter compared to the uncrosslinked groups, since there is considerable water absorption from the 85% isopropyl alcohol solution when the GelMA fibers are soaked before light exposure (Figure S1). Furthermore, TCP particles in TCP-incorporated membranes directly affect the conductivity of the polymer solution,[14,33] acting synergistically toward the increase in charge density on the surface of the spinning jet, leading to a reduction in self-repulsion tension and, consequently, increasing elongation forces and the formation of thinner fibers.[15,33] The SEM images also demonstrated that the TCP particles were distinct in form and size (Figure 1C).

The FTIR spectra of TCP, GelMA/PCL-TCP, GelMA/PCL, GelMA, GelMA-TCP, PCL, and PCL-TCP are shown in Figure 2A. The C–H (~2860 cm^{-1}) and C=O (~1720 cm^{-1}) characteristic stretching peaks correspond to the PCL observed in PCL containing membranes' spectrum. Similar to the previous observation by Janarthanan et al.,[34] the distinct peaks of GelMA include peaks near ~3500–3250 cm^{-1} for OH, ~1640 cm^{-1}, and 1550 cm^{-1} mainly due to the effect of N–H bonds, C=O bonds, and N–H bond wagging, respectively. Moreover, the composite membranes of GelMA/PCL confirm the presence of characteristic peaks for GelMA (1640 cm^{-1}, for the C=C methacrylate group, and 1650 cm^{-1}, for C=O stretching of the amide group) and PCL (3000 cm^{-1} for the C–H hydroxyl group stretching and 1726 cm^{-1} for C=O [ester group] stretching group). The spectra of GelMA/PCL membranes tend to appear as merged peaks of both strong PCL characteristic peaks and mild GelMA peaks, confirming possible interactions and hybrid formation at corresponding regions. Notably, the prominent characteristic peaks of TCP and GelMA/PCL-TCP-incorporated membranes were observed at 920–1033 cm^{-1}, which are mainly attributed to PO_4 and OH stretching. The absorption peak from C=C bonding for TCP at the range of 1600–267 is found for PCL-TCP and GelMA membranes. The

GelMA/PCL-TCP spectrum confirmed an increase in the 1030 cm^{-1} band, which is a strong band assigned to the stretching of PO for HPO_4^{2-} and PO_4^{3-}.

The XRD analyses of TCP, GelMA/PCL-TCP, GelMA/PCL, GelMA, GelMA-TCP, PCL, and PCL-TCP are shown in Figure 2B. XRD spectra of the GelMA sample show a broad hump centered around 22° in the 2-theta range from 10 to 35°, suggesting that GelMA has an amorphous structure. Moreover, TCP is the most basic form of calcium phosphates and displays several peaks, an indexing analysis suggestive of a crystal structure with an orthorhombic phase. At the same time, the pattern of GelMA-TCP can be viewed as a linear combination of 27 wt % TCP and 73 wt % GelMA. In contrast, both PCL-TCP and PCL show two major characteristic peaks around 21.5 and 23.85°. Compared to the above two samples, the two diffraction peaks GelMA/PCL and GelMA/PCL+ 15% TCP shift to 21.7 and 23.9°, respectively. This upshifts to a high angle, suggesting smaller d-spacing and close packing. Based on the Scherrer equation computation, the crystalline sizes of GelMA/PCL and GelMA/PCL-TCP are 56 and 95 nm, respectively. Interestingly, the peak intensity ratio of 21.5 and 23.85° remains the same for PCL-TCP and PCL samples. This ratio significantly decreases for the samples GelMA/PCL and GelMA/PCL-TCP, especially for GMA/PCL-TCP; the peak of around 23.9° is higher than that at 21.7°. Collectively, these data confirm the chemical characteristics of the composite membranes synthesized in the study and suggest that TCP incorporation acts as a nucleant for crystallization.

The energy-dispersive X-ray spectroscopy (EDS) results in Figure 2C confirmed that the pix depicts the distribution of TCP particles in the GelMA/PCL-TCP. Moreover, the thermogravimetric analysis profiles of PCL, PCL-TCP, GelMA, GelMA/PCL, GelMA/PCL-TCP, and GelMA-TCP scaffolds are shown in Figure 2D. As displayed in the thermograms, all scaffold shows a step of degradation at ~100 °C, most probably due to water loss. While the weight loss for PCL-containing groups occurred when the temperature was approximately 420 °C, for GelMa and GelMa-TCP-containing groups, the curve shows a loss of integrity, particularly between 50 and 450 °C, similar to the previously reported results,[26] whereas PCL/GelMa blends and GelMA/PCL-TCP show a thermal behavior similar to PCL. Furthermore, the residual weights at 700 °C were 9.361, 20.13, 22.26, 8.84, 28.29, and 16.14% for PCL, PCL-TCP, GelMA, GelMA/PCL, GelMA-TCP, and GelMA/PCL-TCP, respectively. A slight increase in thermal stability due to the addition of TCP is in agreement with the results reported by Bruyas et al.[35] Altogether, the results validate the composition of the scaffold and the successful incorporation of TCP particles within each TCP-loaded membrane.

Swelling Ratio and In Vitro Degradation Profile.

When creating a membrane for tissue regeneration, swelling is a factor to consider because it affects body fluid absorption, nutrient, and metabolite transport through the material, and it can apply stress on the tissues in its vicinity.[36,37] As expected, PCL membranes had the lowest swelling capacity (~17%) compared to the other groups due to the compound hydrophobicity. The results showed a rapid water uptake within the first hour of GelMA (~200%), GelMA-incorporated membranes (~111%) for GelMA/PCL, and (~100%) GelMA/PCL-TCP (Figure 3A). The swelling profiles showed a steady profile over

the first 24 h of the experimental analysis, mainly attributed to the hydrophilicity of the GelMA-incorporated membranes, which is synergized by the presence of hydrophilic TCP particles.

Obtaining a degradation rate that permits load transfer to the regenerating bone is essential for bone tissue engineering. The results showed no significant weight loss of the PCL membranes (~95%) among all the other groups without a significant effect of adding TCP (Figure 3B). In contrast, GelMA/PCL, GelMATCP, and GelMA/PCL-TCP membranes showed slow and steady degradation profiles for the first 2 weeks and 50% remaining mass after 4 weeks. After 4 weeks, the weight loss of the pure GelMA membranes was found to be 95% compared to its starting weight.

Interestingly, the presence of GelMA significantly increased the degradation profile of the TCP-incorporated membranes, i.e., GelMA/PCL-TCP and GelMA-TCP, compared to PCL-TCP, likely due to enhanced hydrophilicity. This degradation profile of TCP-incorporated membranes is essential to releasing Ca^{2+} and PO_4^{3-} minerals into the surrounding environment, which can provide the necessary elements for bone regeneration.

Contact Angle.

The contact angle is a critical feature of surface wettability, energy, and membrane hydrophilicity. Here, we evaluated the effect of TCP particles and GelMA incorporation on the surface hydrophilicity of the processed membranes (Figure 3C–E). The contact angle of uncrosslinked membranes could not be determined since a water drop was instantly absorbed as it came into contact with the membranes. On the other hand, crosslinked nanofibers and PCL membranes were stable in these settings. As expected, the contact angle values of the PCL membrane (~138°) confirmed the hydrophobic character of matrices. Furthermore, incorporating TCP significantly decreased the contact angle (~120°) and the hydrophobicity. Interestingly, we observed a significant decrease in the contact angle of the composite membrane GelMA/PCL to ~53° and the GelMA membrane (~30°), which supported the hydrophilic characteristics of these membranes. Meanwhile, TCP incorporation on the GelMA/PCL and GelMA groups increased the contact angle of both membranes, ~90 and ~79°, respectively; however, it was still around the hydrophilicity limit, 90°. The increase in CA for TCP-incorporated membranes, i.e., GelMA-TCP and GelMA/PCL-TCP membranes, is attributed to the chemical and morphological properties of the TCP membranes.[38]

Biomechanical Properties.

The biomechanical properties of the membranes (i.e., PCL, PCL-TCP, GelMA, GelMA-TCP, GelMA/PCL, and GelMA/PCL-TCP) were analyzed using a uniaxial tensile test (Figure 3F–H). The tensile strength and Young's modulus were enhanced in the uncrosslinked groups compared to the crosslinked ones without significant differences for the TCP-incorporated groups except in uncrosslinked GelMA/PCL and GelMA membranes. The tensile strength of PCL membranes (~3.6 MPa) was the highest, followed by the GelMA/PCL group (~1.4 MPa), and then GELMA (~0.5 MPa), which was the lowest. Furthermore, we can appreciate the effect of crosslinking on elevating tensile

strength, particularly for the GelMA/PCL-TCP and GelMA groups. The TCP-incorporated membranes had no significant effect on tensile strength for the uncrosslinked GelMA/PCL (~1.17 MPa) and GelMA (~0.8 MPa) groups but significantly decreased in the PCL group (2.64 MPa). Interestingly, TCP increased the tensile strength of crosslinked GelMA/PCL and dropped it for crosslinked GelMA, compared to the uncrosslinked groups.

The elongation at break (%) for the crosslinked GelMA (82%) and GelMA/PCL (95%) membranes is significantly higher than that for the uncrosslinked GelMA (25%) and GelMA/PCL (39%) membranes, and even close to or higher than the PCL (92%) membranes. The GelMA/PCL-TCP group gains a significant enhancement of elongation at break (%) compared to other groups due to the presence of TCP particles, which correlated with increases in overall remembrance rigidity. Notably, GelMA incorporation significantly decreases tensile strength and elongation at break, even after crosslinking, which plays a significant role in improving these properties, most likely due to the weakness and fragility of the gelatin.[38]

In Vitro Cellular Adhesion and Cell Proliferation.

When considering the choice of membrane for use as part of regenerative procedures employing GBR, membrane cytocompatibility is one of the most important considerations.[27] An ideal membrane should have optimal cell affinity and sufficient tissue adhesiveness to achieve successful bone regeneration. Representative fluorescent images (Figure 4A,B) and SEM (Figure 4C) show that aBMSCs seeded on all the membranes displayed typical fibroblast-like extended morphology. Moreover, filopodia were noticed on cells seeded on all the membranes without any significant difference, indicating that all the membranes had suitable cytocompatibility. Likewise, the viability of the aBMSCs (Figure 4D) was investigated by alamarBlue Assay on the different membranes, i.e., TCP and GelMA, PCL, or GelMA/PCL composite. On days 1 and 3, there were no significant differences among all the groups. However, the GelMA/PCL-TCP membrane showed the highest viability on 5 and 7 days. This agrees with previous findings, where the GelMA/TCP composite showed higher human adipose-derived stem cell (hASC) viability than GelMA.[29] Altogether, data confirmed that GelMA/PCL-TCP has high biocompatibility and the potential to promote superior cell infiltration, nutrition, and tissue formation.

In Vitro Biomineralization Nodule Quantification and Osteogenic Differentiation of aBMSCs.

GBR membranes should minimally exhibit the capacity to support mineralization and ideally exhibit the ability to promote osteogenic differentiation of resident host cells upon implantation to further bone regeneration.[27] Here, we assessed the potential of the membranes to initiate aBMSC osteogenic differentiation in vitro (Figure 4). After 21 days of culture, mineralization was evaluated by micro-CT (Figure 4E,F). Considering the osteoconductive effect of TCP, mineralization nodule quantification was acquired by the bone volume value of the membranes with cells subtracting the value without cells, using the same threshold for all samples. PCL showed minor mineralization after 21 days. In contrast, TCP-incorporated membranes, i.e., GelMA/PCL-TCP and GelMA-TCP, significantly enhanced mineralization.

In addition, the expression of ALP, RUNX2, COL 1, and OPN osteogenic genes was further investigated (Figure 5). The data showed that the presence of TCP significantly promoted the osteogenic differentiation of aBMSCs in GelMA/PCL-TCP and GelMA-TCP. This can be due to hydrolysis of the TCP, resulting in the release of Ca^{2+} and HPO_4^-, which, in turn, drives the osteogenic differentiation of aBMSCs.[39] However, the function of TCP-incorporated PCL was inconspicuous compared with others, most likely due to the low degradation rate of PCL. After 7 and 14 days of osteogenic induction, both GelMA/PCL-TCP and GelMA-TCP revealed significantly higher ALP, Runx2, Col1, and OCN expression than others. Moreover, the expression of Runx2, Col1, and OCN, which are crucial late-stage osteogenesis markers, was superior in GelMA/PCL-TCP, compared to GelMA-TCP after 21 days.

In Vivo Bone Tissue Regeneration.

The reconstructed defect area is shown in Figure 6A. The micro-CT revealed a significantly higher bone volume (BV) formation in the critical-size defect area for the GelMA-PCL and GelMA-PCL/TCP groups compared to empty and PCL groups, 10.25 mm^3 ± 3.49 and 13.42 mm^3± 2.85, respectively (Figure 6B–D). The ratio of space occupied by the mineralized bone in the defect space was significantly higher than the empty defect for the three membranes employed, reaching 37.29% ± 6.04 for the GelMA/PCL-TCP group. From the HE and Masson's qualitative staining shown in Figure 7A,B, we observed that the membranes were kept well positioned above the defect area until the end of the experiment, with minimal degradation observed, mainly due to the presence of PCL. Empty defects showed very little newly formed bone with a thick organized connective tissue in the defect area. The PCL membrane yielded modest bone formation starting from the margins of the critical defect area with abundant blood vessel presence. The GelMA/PCL and GelMA/PCL-TCP membranes were observed to promote bone formation throughout the entire defect, with the GelMA/PCL-TCP group exhibiting a higher degree of bone maturity and density as compared to the GelMA/PCL group. The greater maturity and density of the bone in the GelMA/PCL-TCP group was attributed to several factors, including higher mineralization levels (noted through the different eosin staining levels), an increased number of organized and mature osteocytes, the formation of blood vessels leading to improved nutrient flow, and an improved microarchitecture. These collective improvements result in increased mechanical strength and stiffness, indicating that the GelMA/PCL-TCP group may be better suited for clinical applications requiring higher loadbearing capabilities. Our results are in accordance with a previous report that also demonstrated the potential of beta-TCP to improve and accelerate bone formation in critical-sized defects.[40]

Evaluating the bone immunohistochemical markers (Figure 8), we noted a similar expression pattern for Runt-related transcription factor 2 (Runx2) and osteopontin (OPN) in the empty, PCL, and GelMA/PCL groups, with the GelMA/PCL-TCP showing a notable high immunolabeling right beneath the membrane position. Runx2, first detected in preosteoblasts, is an essential transcription factor required for the determination of the osteoblast lineage, evoking the differentiation of multipotent mesenchymal cells into immature osteoblasts and conducting the formation of immature new bone,[41] and OPN, also referred to as bone sialoprotein 1, is secreted by both macrophages and osteoblast-lineage

cells, specifically at the margins of the wound that binds the newly repaired formed bone with the existing bone,[42] both of them being crucial proteins for wound healing.

Regarding the assessment of angiogenesis, which is a critical process for bone formation, we observed a higher expression of cluster of differentiation 31 (CD31), also named as platelet endothelial cell adhesion molecule 1 (PECAM1), and von Willebrand factor (VWF) in the empty defect, probably due to a presence of an organized soft tissue and earlier stages of bone formation. In addition, GelMA/PCL-TCP presented more pronounced immunolabeling for the two markers, agreeing with the ability of calcium phosphates to promote and improve appropriate vascularization.[43] The VWF, synthesized by endothelial cells, carries the coagulation factor VIII and regulates angiogenesis through multiple cross-talking extracellular and intracellular pathways that converge to regulate vascular endothelial growth factor receptor-2 (VEGFR2);[44] moreover, CD31/PECAM1 is constitutively expressed on all vascular cells and is another well-defined immunohistochemical marker of blood vessels.[45,46] The suitable immunolabeling identified for these two proteins in the GelMA/PCL-TCP group is noteworthy since de novo angiogenesis is vital for the critical-sized bone defect to heal and achieve homeostasis.

CONCLUSIONS

Here, we described the development of a GelMA/PCL-TCP composite membrane. The membrane provides tunable properties, which improve bioactivity and offer stable mechanical characteristics. Morphological investigation indicated that TCP particles are integrated within GelMA/PCL composite membrane microfibers. The membrane exhibited improved thermal stability and degradation profile in vitro compared to PCL and GelMA/PCL counterpart membranes. Moreover, GelMA/PCL-TCP composite fibrous membranes were biocompatible, showed improved cell-to-cell and cell-to-matrix intercommunication and promoted osteogenesis. In vivo experiments demonstrated that the GelMA/PCL-TCP composite membrane induced the formation of new bone. The results underscore the potential of GelMA/PCL-TCP composite membranes to be used in the context of guided tissue and bone regenerative procedures.

MATERIALS AND METHODS

GelMA Synthesis and Preparation.

GelMA was synthesized following the previously described method.[47] In brief, gelatin type A derived from porcine skin (Sigma-Aldrich, St. Louis, Missouri, USA) (10% w/v) was dissolved in DPBS on a heating plate at 50 °C. Next, 0.8 mL of methacrylic anhydride (Sigma-Aldrich) per 1 g of gelatin was introduced into the gel solution to initiate a methacrylation reaction for 2 h under stirring conditions. An equal amount of warm DPBS was added to the solution to stop the reaction. Finally, the mixture was dialyzed in deionized (DI) water using 12–14 kDa porous membrane tubing (Spectrum Spectra/Por, Fisher Scientific International Inc., Hampton, New Hampshire, USA) at 45 ± 5 °C for 7 days to remove solution impurities. The prepared solution was frozen at −80 °C overnight and then freeze-dried for 7 days (Labconco FreeZone 2.5 L, Labconco Corporation, Kansas City, Missouri, USA). The formed white porous foam was stored at −20 °C until further use.

Preparation of Electrospun Membranes.

GelMA and PCL were individually dissolved in acetic acid (Thermo Fisher Scientific, Inc., Waltham, Massachusetts, USA) and hexafluoro-2-propanol (HFP) (Sigma-Aldrich) to obtain 150 and 100 mg/mL solutions, respectively. Then, equal amounts of GelMA and PCL solution were mixed under continuous stirring to form a 50:50 (v/v) polymer blend.

For the preparation of the osteoconductive membrane, β-TCP with an average particle size of 100 nm (Berkeley Advanced Biomaterials Inc., Berkeley, California, USA) was added to the GelMA/PCL blend, pure GelMA, and pure PCL groups at 15% (wt/wt) concentration. TCP-containing scaffolds were prepared as follows: TCP particles were added to GelMA/PCL (50:50) blend, GelMA, and PCL solutions; they were then sonicated for 90 min to ensure good particle dispersion. The prepared membrane groups were named PCL, PCL-TCP, GelMA, GelMA-TCP, and GelMA/PCL-TCP. The crosslinking agent, lithium phenyl(2,4,6-trimethylbenzoyl)phosphinate (LAP) (TCI America Inc., Portland, Oregon, USA), was added to the GelMA-containing groups at a concentration of 0.075% (w/v). The membranes were processed via electrospinning (Table 1). Briefly, the solutions were loaded into a plastic syringe (Becton, Dickson and Company, Franklin Lakes, New Jersey, USA) connected to stainless-steel needles (CML Supply LLC, Lexington, Kentucky, USA.). Next, the solutions were pumped at a high-voltage source (ES50P-10 W/DAM, Gamma High-Voltage Research, Inc., Ormond Beach, Florida, USA) over a grounded stainless-steel collecting drum (ϕ = 4 cm). The processed membranes were collected directly onto an aluminum-foil-covered rotating mandrel at room temperature (RT) and 18% relative humidity.

The electrospun mats were kept in a vacuum desiccator oven for 2 days to remove any residual solvent. The fibrous mats were cut into the desired size and length based on the required experiment, wetted with isopropyl alcohol (85%), gently dried with Kimwipes (Kimberly-Clark Corporation, Irving, Texas, USA), and light-cured for 5 min on each side using Light Zone II (BesQual-E300N, Meta Dental Corp, Glendale, New York, USA) for cross-linking.

Morphological, Chemical, and Thermal Characterizations.

The morphological assessment of the processed electrospun membranes (uncrosslinked and crosslinked fibrous membranes) was examined via scanning electron microscopy (Tescan MIRA3 FEGSEM, Tescan USA Inc., Warrendale, Pennsylvania, USA). Prior to imaging, the membranes were mounted on AI stubs and sputter-coated with Au (SPI-Module Carbon/Sputter coater, Thermo Fisher Scientific Inc.). The average fiber diameter (AFD) was analyzed from three different images at the same magnification using ImageJ software (National Institutes of Health, Bethesda, Maryland, USA). The results are calculated as average ± standard deviation.

Fourier transform infrared spectroscopy in the attenuated total reflection mode (ATR-FTIR, Nicolet iS50, Thermo Fisher Scientific, Inc.) was used to characterize the presence of specific chemical groups of GelMA, PCL, and GelMA/PCL, and their interaction of TCP particles. Sixteen scans were analyzed between 4000 and 600 cm^{-1} at 4 cm^{-1} resolution.

The EDS (Kratos Axis Ultra XPS) was used to assess the elemental composition of TCP-incorporated electrospun membranes. The structure and phase content of PCL, PCL-TCP, GelMA, GelMA-TCP, and GelMA/PCL-TCP were examined by XRD using Cu K (λ = 1.5406 Å) in Bragg–Brentano geometry on a Rigaku Ultima IV diffractometer (Rigaku Americas Corporation, Woodlands, Texas, USA). The X-ray source and detector were connected to a scan of 2-theta (2) ranging from 5 to 45° with 0.05° steps at a scan speed of 2° min^{-1}.

The thermal characteristics of PCL, PCL-TCP, GelMA, GelMATCP, and GelMA/PCL-TCP scaffolds were examined by thermogravimetric analysis (TGA, Perkin Elmer TGA 7, Perkin-Elmer Inc.). The samples were heated to 800 °C at a rate of 40 °C min^{-1} and in a nitrogen atmosphere.

Biomechanical Properties.

In order to evaluate the mechanical properties, membrane tear resistance (n = 4 per group) was assessed for uncrosslinked and crosslinked membranes using uniaxial tensile testing (eXpert 5601, ADMET, Inc., Norwood, Massachusetts, USA). The samples were cut into a rectangular shape (25 mm × 3 mm), and the thickness was measured (Mitutoyo Digimatic Caliper; Mitutoyo Corporation, Tokyo, Japan) at three distinct positions to obtain an average thickness for each analyzed sample. Testing was carried out at a crosshead speed of 1 mm min^{-1}. Three distinct mechanical properties, Young's modulus, elongation at break, and tensile strength, were acquired from the load-position curves and reported in MPa.[14]

Surface Energy and Contact Angle Determinations.

The samples (n = 3 per group) were cut (1 × 1 cm^2) and fixed on the glass slide using double-sided carbon tape to ensure their complete flatness. The angle at which a liquid/vapor interface meets a solid surface is known as θ. The liquid is considered to moisten the solid if the angle θ is less than 90°. It is termed as non-wetting if it is greater than 90°. Complete wetting is represented by a contact angle of zero. In the case of water, the lower the number, the more hydrophilic the solid surface.[48] A Ramé-Hart goniometer software (ramé-hart instrument co., Succasunna, New Jersey, USA) was used to measure the contact angle between the prepared membrane surfaces and water drops. A drop of water (0.1 mL) was applied on the membrane surfaces with a BD ultrafine syringe of 0.5 mL (Becton Dickinson and Company, Franklin Lakes, New Jersey, USA). Images of the drop were analyzed to provide each sample's values of contact angles.

In Vitro Dimensional Stability and Swelling Properties.

The developed membranes (n = 3 per group) were cut into squares (1 × 1 cm^2). The original weight for each sample was taken, and then the samples were incubated at 37 °C in 2 mL of DPBS containing collagenase type A (1 U/mL) for 28 days. At predetermined time points, the samples were washed twice with distilled water. Then, the samples were allowed to dry at RT for 24 h before dried weight measurement. Dimensional stability, namely, shrinkage ratios of the electrospun membranes before and after incubation in collagenase medium, was used to obtain shrinkage rates for each sample.

The formula calculated the degradation ratio: the remaining mass $(\%) = \frac{W_d}{W_o} \times 100$ (where W_d is the dry weight at a different time point and W_o is the initial original weight).

Swelling capacity was calculated after soaking the membranes in PBS solution for 24 h and measured over 1, 3, 6, and 24 h. The following formula was used: swelling capacity $(\%) = \frac{W_t - W_0}{W_0} \times 100$ (where W_t is the wet weight after soaking and W_o is the original weight).

Cell Culture.

Alveolar bone-derived mesenchymal stem cells (aBMSCs) previously isolated and characterized for $CD90^+$, $CD73^+$, and $CD105^+$ were used for all reported in vitro experiments.[49] Cells were cultured in alpha minimum essential medium (α-MEM; Gibco Invitrogen Corporation, Grand Island, New York, USA) with 15% fetal bovine serum (FBS; Gibco Invitrogen Corporation), 1% antibiotic/antimycotic, and 1% ascorbic acid (AA) at 37 °C and a 5% CO_2 incubator.

Cell–Membrane Interaction.

Briefly, after crosslinking, 1 cm × 1 cm membranes ($n = 3$ per group) were disinfected under UV light for 30 min and placed into a 24-well plate. aBMSCs at passage 6 were seeded on the membranes at a density of 3×10^3 cells/well and cultured for 12 h, 24 h, and 7 days to observe the cell–membrane interaction. Subsequently, the membranes were washed in PBS and fixed with 4% paraformaldehyde (PFA) for 30 min at RT. Then, 12 and 24 h samples were stained with F-action (Invitrogen ActinGreen 488 ReadyProbes Reagent, Thermo Fisher Scientific, Inc., 15 min) and DAPI (5 min). Images were captured by the fluorescence microscope (Nikon Eclipse 50i, Japan). On the other side, 7 day samples were dehydrated in gradient ascending ethanol (70, 80, 90, and 100%, 15 min each). Then, the samples were incubated in hexamethyldisilazane (HMDS, Sigma-Aldrich) overnight. The samples were then sputtered with gold prior to SEM imaging (Tescan MIRA 3 FEG-SEM).

Cell Proliferation.

After crosslinking, 1.5 cm × 1.5 cm membranes ($n = 4$ per group) were mounted on sterile cell crowns (CellCrown, Scaffdex Ltd., Tampere, Finland). aBMSCs at passage 6 were harvested and seeded at a density of 3×10^3 cells/well in a volume of 500 μL medium. alarmarBlue Cell Viability Assay (Invitrogen Corporation, Carlsbad, California, USA) was performed for cell proliferation evaluation at 1, 3, 5, and 7 days. Briefly, 50 μL of alamarBlue Cell Viability Reagent was added to each well and incubated for 3 h at 37 °C at each time point. Then, 100 μL of reagent from the well was transferred into a 96-well plate in triplicate, and the fluorescence was determined at excitation 530 nm and emission 590 nm by SpectraMax iD3 microplate readers (Molecular Devices LLC, San Jose, California, USA). Finally, each well was washed with PBS and a new fresh media was introduced.

Mineralization Nodule Quantification.

aBMSCs at 5×10^4 cells/well were seeded on each membrane and cultured in the osteogenic induction medium (α-MEM + 15% FBS + 1% antibiotic +10 mM β-glycerol phosphate +100 nM dexamethasone + 50 mg/mL ascorbic acid) for 14 and 21 days.

The membranes were imaged by μCT using high-definition parameters (45 kV, 133 μA, and 10 μm voxel sizes) for mineralization nodule quantification after 21 days of culture. Cell-free membranes were imaged in air, and cell-containing membranes were in phosphate-buffered saline (PBS, Sigma-Aldrich). The images were collected over 360° every 0.3°, with three images collected for each step and averaged to reduce noise. The images were reconstructed and analyzed with a program provided by the manufacturer (Scanco μCT 100 Medical AG, SCANCO Medical AG, Brüttisellen, Switzerland) using a global threshold for bone formation detection, which made it possible to segment membrane and mineralization nodules. The mineralization nodule quantification was acquired by the bone value of the membranes with cells subtracting the value without cells.[50]

Real-Time PCR.

A quantitative polymerase chain reaction (qPCR) evaluated the osteogenic gene expression after 7, 14, and 21 days. In brief, the total RNA was isolated from harvested cells by TRIzol Reagent (Invitrogen Corporation, Carlsbad, California, USA) and purified by TRIzol Plus RNA Purification Kit and Phasemaker Tubes Complete System (Invitrogen Corporation). Then, RNA was reversed to cDNA by SuperScript II Reverse Transcriptase (Invitrogen Corporation). Real-time polymerase chain reaction (RT-PCR) was performed by TaqMan Gene Expression Master Mix (Thermo Fisher Scientific, Inc.) to evaluate the osteogenic gene expression of alkaline phosphatase (ALP, Hs01029144_m1), Runt-related transcription factor 2 (Runx2, Hs01047973_m1), collagen alpha 1 (COL1A1, Hs00164004_m1), and osteocalcin (OCN, Hs01587814_g1). Glyceraldehyde 3-phosphate dehydrogenase (GAPDH, Hs02758991_g1) was used as the housekeeping gene. The relative gene expression was calculated using the $2^{-\Delta\Delta CT}$ method.

In Vivo Bone Tissue Regeneration.

After considering the mechanical results of the crosslinked GelMA-TCP group in comparison to PCL-based membranes, we have concluded that this material may not offer the necessary strength required to hind soft tissue invasion into the injured site for effective bone regeneration. Therefore, we excluded it from further in vivo investigation. For that, 24 6-week-old male Fischer 344 rats (Envigo RMS, Inc., Oxford, Michigan, USA) weighing about 250 g were used to determine the regenerative potential of the GelMA-PCL fibers modified with beta-TCP. The procedures were performed according to previous studies.[27,51,52] Briefly, a single 6 mm-diameter calvarial defect using a trephine bur with a 6.95 mm outside diameter and a 6.0 mm inside diameter (REF 04948501, Ace Surgical Supply Co., Brockton, Massachusetts, USA) was done, and the animals were randomly assigned to four groups, namely, according to the received membrane: empty, PCL, GelMA/PCL, and GelMA/PCL-TCP. The animals were euthanized 6 weeks after surgery by CO_2 inhalation, and the skulls were collected and fixed in 4% PFA (Sigma-Aldrich).

Micro-Computed Tomography (Micro-CT).

Scanco CT 100 (Scanco Medical AG, Brüttisellen, Switzerland) equipment was used to examine the newly formed bone at the critical-defect location. The following scan parameters were used: 70 kV, 114 μA monochromatic X-rays, and 25 μm voxel sizes were used to create a 360° rotation. The exposure period was kept to an average of 500 ms per frame. For 3D image reconstruction, the Scanco Medical System software was employed. The 3D image was then utilized to trace the original defects circumferentially, which was named the region of interest (ROI) afterward. Each sample's ROI was examined for total volume (TV, mm^3), BV (mm^3), and the ratio of the segmented BV to the total volume of the region of interest (BV/TV, %).

Immunohistology Analysis.

Following micro-CT, the calvaria samples were decalcified in 10% EDTA for 4 weeks. Subsequently, the samples were histologically processed to be paraffin-embedded. Histological sections (4 μm thick) were stained with hematoxylin and eosin (HE) and Masson's trichrome (MT). To examine soft and mineralized tissue neoformation, the slides were imaged using a High Capacity Digital Pathology Slide Scanner (Aperio GT 450, Leica Biosystems, Deer Park, Illinois, USA) at 2×, 4×, and 10×. For immunostaining, sections were dewaxed at 60 °C for 15 min, rehydrated using well-established ethanol gradients, and then incubated for 20 min in 3% at RT to decrease the activity of endogenous peroxidase. Later, the slides were incubated (10 min) in 3% bovine serum albumin (BSA) at RT to block unspecific binding. After that, the antibodies for bone formation evaluation, anti-osteopontin (Rabbit polyclonal, ab216402, Abcam, Cambridge, Massachusetts, USA), anti-RUNX2 (Rabbit monoclonal, ab92336, Abcam), and for angiogenesis evaluation, anti-CD31/PECAM1 (00055, Fortis Life Sciences, Waltham, Massachusetts, USA) and anti-Factor VIII Related Antigen/von Willebrand Factor (RB281A, Epredia, Portsmouth, New Hampshire, USA), were applied overnight at 4 °C. Subsequently, the sections were incubated with Goat Anti-Mouse IgG H&L (Alexa Fluor 488, ab6785, Abcam) at dilution 1:200 for 1 h at RT. Cell nuclei were stained with DAPI using VECTASHIELD Antifade mounting media. The images were acquired with a microscope (ECHO Revolve, BICO Company, San Diego, California, USA) at 10×, and the positive immunofluorescence staining areas were quantified from six randomly selected images per group using ImageJ software (National Institutes of Health).[53]

Statistical Analysis.

All experiments were repeated three times in triplicate. Results were presented as mean ± standard deviation (SD). One-way ANOVA or two-way ANOVA in multiple comparisons was used to determine statistical significance between the different groups using Prism 8.0 software (GraphPad Software, San Diego, California, USA). Statistical significance was considered at $p < 0.05$.

Supplementary Material

Refer to Web version on PubMed Central for supplementary material.

ACKNOWLEDGMENTS

M.C.B. acknowledges the National Institutes of Health (NIH – National Institute of Dental and Craniofacial Research, grant R01DE031476). D.K. acknowledges NIH/NIDCR, grant R01DE028657). The content is solely the responsibility of the authors and does not necessarily represent the official views of the NIH and the National Science Foundation (NSF). J.M. acknowledges the funding from the Gravitation Program “Materials Driven Regeneration”, funded by the Netherlands Organization for Scientific Research (024.003.013).

REFERENCES

(1). Cho YD; Kim KH; Lee YM; Ku Y; Seol YJ Periodontal Wound Healing and Tissue Regeneration: A Narrative Review. Pharmaceuticals 2021, 14, 456. [PubMed: 34065862]

(2). Kwon T; Lamster IB; Levin L Current Concepts in the Management of Periodontitis. Int. Dent. J. 2021, 71, 462–476. [PubMed: 34839889]

(3). Tariq M; Iqbal Z; Ali J; Baboota S; Talegaonkar S; Ahmad Z; Sahni JK Treatment Modalities and Evaluation Models for Periodontitis. Int. J. Pharm. Invest. 2012, 2, 106–122.

(4). Eke PI; Thornton-Evans GO; Wei L; Borgnakke WS; Dye BA; Genco RJ Periodontitis in Us Adults: National Health and Nutrition Examination Survey 2009–2014. J. Am. Dent. Assoc. 2018, 149, 576–588.e6. [PubMed: 29957185]

(5). Cobb CM; Sottosanti JS A Re-Evaluation of Scaling and Root Planing. J. Periodontol. 2021, 92, 1370–1378. [PubMed: 33660307]

(6). Mitani A; Takasu H; Horibe T; Furuta H; Nagasaka T; Aino M; Fukuda M; Fujimura T; Mogi M; Noguchi T Five-Year Clinical Results for Treatment of Intrabony Defects with Emd, Guided Tissue Regeneration and Open-Flap Debridement: A Case Series. J. Periodontal Res. 2015, 50, 123–130. [PubMed: 24815103]

(7). Crea A; Deli G; Littarru C; Lajolo C; Orgeas GV; Tatakis DN Intrabony Defects, Open-Flap Debridement, and Decortication: A Randomized Clinical Trial. J. Periodontol. 2014, 85, 34–42. [PubMed: 23537123]

(8). Hanes PJ Bone Replacement Grafts for the Treatment of Periodontal Intrabony Defects. Oral Maxillofac. Surg. Clin. North Am. 2007, 19, 499–512. [PubMed: 18088901]

(9). Chu C; Zhao X; Rung S; Xiao W; Liu L; Qu Y; Man Y Application of Biomaterials in Periodontal Tissue Repair and Reconstruction in the Presence of Inflammation under Periodontitis through the Foreign Body Response: Recent Progress and Perspectives. J. Biomed. Mater. Res., Part B 2022, 110, 7–17.

(10). Sasaki JI; Abe GL; Li A; Thongthai P; Tsuboi R; Kohno T; Imazato S Barrier Membranes for Tissue Regeneration in Dentistry. Biomater. Invest. Dent. 2021, 8, 54–63.

(11). Gamal AY; Iacono VJ Enhancing Guided Tissue Regeneration of Periodontal Defects by Using a Novel Perforated Barrier Membrane. J. Periodontol. 2013, 84, 905–913. [PubMed: 23003916]

(12). Aytac Z; Dubey N; Daghrery A; Ferreira JA; de Souza Araújo IJ; Castilho M; Malda J; Bottino MC Innovations in Craniofacial Bone and Periodontal Tissue Engineering - from Electrospinning to Converged Biofabrication. Int. Mater. Rev. 2022, 67, 347–384. [PubMed: 35754978]

(13). Rowe MJ; Kamocki K; Pankajakshan D; Li D; Bruzzaniti A; Thomas V; Blanchard SB; Bottino MC Dimensionally Stable and Bioactive Membrane for Guided Bone Regeneration: An in Vitro Study. J. Biomed. Mater. Res., Part B 2016, 104, 594–605.

(14). Mü EA; Albuquerque MTP; Zero B; Kamocki K; Piva E; Gregory RL; Bottino MC Development and Characterization of Novel Zno-Loaded Electrospun Membranes for Periodontal Regeneration. Dent. Mater. 2015, 31, 1038–1051. [PubMed: 26116414]

(15). Bottino MC; Thomas V; Schmidt G; Vohra YK; Chu TM; Kowolik MJ; Janowski GM Recent Advances in the Development of Gtr/Gbr Membranes for Periodontal Regeneration–a Materials Perspective. Dent. Mater. 2012, 28, 703–721. [PubMed: 22592164]

(16). Bottino MC; Thomas V; Janowski GM A Novel Spatially Designed and Functionally Graded Electrospun Membrane for Periodontal Regeneration. Acta Biomater. 2011, 7, 216–224. [PubMed: 20801241]

(17). Ahmed FE; Lalia BS; Hashaikeh R A Review on Electrospinning for Membrane Fabrication: Challenges and Applications. Desalination 2015, 356, 15–30.

(18). Zafar M; Najeeb S; Khurshid Z; Vazirzadeh M; Zohaib S; Najeeb B; Sefat F Potential of Electrospun Nanofibers for Biomedical and Dental Applications. Materials 2016, 9, 73. [PubMed: 28787871]

(19). Zhang Y; Ouyang H; Lim CT; Ramakrishna S; Huang ZM Electrospinning of Gelatin Fibers and Gelatin/Pcl Composite Fibrous Scaffolds. J. Biomed. Mater. Res., Part B 2005, 72, 156–165.

(20). Binulal NS; Natarajan A; Menon D; Bhaskaran VK; Mony U; Nair SV Pcl-Gelatin Composite Nanofibers Electrospun Using Diluted Acetic Acid-Ethyl Acetate Solvent System for Stem Cell-Based Bone Tissue Engineering. J. Biomater. Sci., Polym. Ed. 2014, 25, 325–340. [PubMed: 24274102]

(21). Ren K; Wang Y; Sun T; Yue W; Zhang H Electrospun Pcl/Gelatin Composite Nanofiber Structures for Effective Guided Bone Regeneration Membranes. Mater. Sci. Eng. C 2017, 78, 324–332.

(22). Causa F; Netti PA; Ambrosio L; Ciapetti G; Baldini N; Pagani S; Martini D; Giunti A Poly-Epsilon-Caprolactone/Hydroxyapatite Composites for Bone Regeneration: In Vitro Characterization and Human Osteoblast Response. J. Biomed. Mater. Res., Part A 2006, 76, 151–162.

(23). Fujihara K; Kotaki M; Ramakrishna S Guided Bone Regeneration Membrane Made of Polycaprolactone/Calcium Carbonate Composite Nano-Fibers. Biomaterials 2005, 26, 4139–4147. [PubMed: 15664641]

(24). Dong Z; Yuan Q; Huang K; Xu W; Liu G; Gu Z Gelatin Methacryloyl (Gelma)-Based Biomaterials for Bone Regeneration. RSC Adv. 2019, 9, 17737–17744. [PubMed: 35520570]

(25). Yang F; Both SK; Yang X; Walboomers XF; Jansen JA Development of an Electrospun Nano-Apatite/Pcl Composite Membrane for Gtr/Gbr Application. Acta Biomater. 2009, 5, 3295–3304. [PubMed: 19470413]

(26). Choi J-B; Kim Y-K; Byeon S-M; Park J-E; Bae T-S; Jang Y-S; Lee M-H Fabrication and Characterization of Biodegradable Gelatin Methacrylate/Biphasic Calcium Phosphate Composite Hydrogel for Bone Tissue Engineering. Nanomaterials 2021, 11, 617. [PubMed: 33801249]

(27). Dubey N; Ferreira JA; Daghrery A; Aytac Z; Malda J; Bhaduri SB; Bottino MC Highly Tunable Bioactive Fiber-Reinforced Hydrogel for Guided Bone Regeneration. Acta Biomater. 2020, 113, 164–176. [PubMed: 32540497]

(28). Chen CM; Chen SM; Lin SF; Liang HC; Wu CC Clinical Efficacy of Polycaprolactone Beta-Calcium Triphosphate Composite for Osteoconduction in Rabbit Bone Defect Model. Polymer 2021, 13, 2552.

(29). Lee S; Choi D; Shim JH; Nam W Efficacy of Three-Dimensionally Printed Polycaprolactone/Beta Tricalcium Phosphate Scaffold on Mandibular Reconstruction. Sci. Rep. 2020, 10, 4979. [PubMed: 32188900]

(30). Bohner M; Santoni BLG; Döbelin N β-Tricalcium Phosphate for Bone Substitution: Synthesis and Properties. Acta Biomater. 2020, 113, 23–41. [PubMed: 32565369]

(31). Daghrery A; Bottino MC Advanced Biomaterials for Periodontal Tissue Regeneration. Genesis 2022, 60, No. e23501. [PubMed: 36113074]

(32). Siqueira L; Passador FR; Costa MM; Lobo AO; Sousa E Influence of the Addition of Beta-Tcp on the Morphology, Thermal Properties and Cell Viability of Poly (Lactic Acid) Fibers Obtained by Electrospinning. Mater. Sci. Eng. C 2015, 52, 135–143.

(33). Oraby MA; Waley AI; El-Dewany AI; Saad EA; El-Hady MA Electrospun Gelatin Nanofibers: Effect of Gelatin Concentration on Morphology and Fiber Diameters. J. Appl. Sci. Res. 2013, 9, 534.

(34). Janarthanan G; Kim IG; Chung EJ; Noh I Comparative Studies on Thin Polycaprolactone-Tricalcium Phosphate Composite Scaffolds and Its Interaction with Mesenchymal Stem Cells. Biomater. Res. 2019, 23, 1. [PubMed: 30788137]

(35). Bruyas A; Lou F; Stahl AM; Gardner M; Maloney W; Goodman S; Yang YP Systematic Characterization of 3d-Printed Pcl/Beta-Tcp Scaffolds for Biomedical Devices and Bone Tissue

Engineering: Influence of Composition and Porosity. J. Mater. Res. 2018, 33, 1948–1959. [PubMed: 30364693]

(36). Ezati M; Safavipour H; Houshmand B; Faghihi S Development of a Pcl/Gelatin/Chitosan/Beta-Tcp Electrospun Composite for Guided Bone Regeneration. Prog. Biomater. 2018, 7, 225–237. [PubMed: 30242739]

(37). Mad Jin R; Sultana N; Baba S; Hamdan S; Ismail AF Porous Pcl/Chitosan and Nha/Pcl/Chitosan Scaffolds for Tissue Engineering Applications: Fabrication and Evaluation. J. Nanomater. 2015, 2015, 1–8.

(38). Lobo AO; Afewerki S; de Paula MMM; Ghannadian P; Marciano FR; Zhang YS; Webster TJ; Khademhosseini A Electrospun Nanofiber Blend with Improved Mechanical and Biological Performance. Int. J. Nanomed. 2018, Volume 13, 7891–7903.

(39). Kwon S-H; Jun Y-K; Hong S-H; Kim H-E Synthesis and Dissolution Behavior of B-Tcp and Ha/B-Tcp Composite Powders. J. Eur. Ceram. Soc. 2003, 23, 1039–1045.

(40). Tebyanian H; Norahan MH; Eyni H; Movahedin M; Mortazavi SJ; Karami A; Nourani MR; Baheiraei N Effects of Collagen/Beta-Tricalcium Phosphate Bone Graft to Regenerate Bone in Critically Sized Rabbit Calvarial Defects. J. Appl. Biomater. Funct. Mater. 2019, 17, 2280800018820490. [PubMed: 30832532]

(41). Komori T Regulation of Proliferation, Differentiation and Functions of Osteoblasts by Runx2. Int. J. Mol. Sci. 2019, 20, 1694. [PubMed: 30987410]

(42). McKee MD; Pedraza CE; Kaartinen MT Osteopontin and Wound Healing in Bone. Cells Tissues Organs 2011, 194, 313–319. [PubMed: 21576907]

(43). Malhotra A; Habibovic P Calcium Phosphates and Angiogenesis: Implications and Advances for Bone Regeneration. Trends Biotechnol. 2016, 34, 983–992. [PubMed: 27481474]

(44). Randi AM; Laffan MA Von Willebrand Factor and Angiogenesis: Basic and Applied Issues. J. Thromb. Haemostasis 2017, 15, 13–20. [PubMed: 27778439]

(45). DeLisser HM; Christofidou-Solomidou M; Strieter RM; Burdick MD; Robinson CS; Wexler RS; Kerr JS; Garlanda C; Merwin JR; Madri JA; et al. Involvement of Endothelial Pecam-1/Cd31 in Angiogenesis. Am. J. Pathol. 1997, 151, 671–677. [PubMed: 9284815]

(46). Park S; Sorenson CM; Sheibani N Pecam-1 Isoforms, Enos and Endoglin Axis in Regulation of Angiogenesis. Clin. Sci. 2015, 129, 217–234.

(47). Ribeiro JS; Münchow EA; Bordini EAF; Rodrigues NS; Dubey N; Sasaki H; Fenno JC; Schwendeman S; Bottino MC Engineering of Injectable Antibiotic-Laden Fibrous Microparticles Gelatin Methacryloyl Hydrogel for Endodontic Infection Ablation. Int. J. Mol. Sci. 2022, 23, 971. [PubMed: 35055155]

(48). Wongwitwichot P; Kaewsrichan J; Chua KH; Ruszymah BH Comparison of Tcp and Tcp/Ha Hybrid Scaffolds for Osteoconductive Activity. Open Biomed. Eng. J. 2010, 4, 279–285. [PubMed: 21625376]

(49). Mason S; Tarle SA; Osibin W; Kinfu Y; Kaigler D Standardization and Safety of Alveolar Bone-Derived Stem Cell Isolation. J. Dent. Res. 2014, 93, 55–61. [PubMed: 24170370]

(50). Persson M; Lehenkari PP; Berglin L; Turunen S; Finnilä MAJ; Risteli J; Skrifvars M; Tuukkanen J Osteogenic Differentiation of Human Mesenchymal Stem Cells in a 3d Woven Scaffold. Sci. Rep. 2018, 8, 10457. [PubMed: 29993043]

(51). Bordini EAF; Ferreira JA; Dubey N; Ribeiro JS; de Souza Costa CA; Soares DG; Bottino MC Injectable Multifunctional Drug Delivery System for Hard Tissue Regeneration under Inflammatory Microenvironments. ACS Appl. Bio Mater. 2021, 4, 6993–7006.

(52). Dubey N; Ferreira JA; Malda J; Bhaduri SB; Bottino MC Extracellular Matrix/Amorphous Magnesium Phosphate Bioink for 3d Bioprinting of Craniomaxillofacial Bone Tissue. ACS Appl. Mater. Interfaces 2020, 12, 23752–23763. [PubMed: 32352748]

(53). Subbiah R; Lin EY; Athirasala A; Romanowicz GE; Lin ASP; Califano JV; Guldberg RE; Bertassoni LE Engineering of an Osteoinductive and Growth Factor-Free Injectable Bone-Like Microgel for Bone Regeneration. Adv. Healthcare Mater. 2023, 12, e2200976.

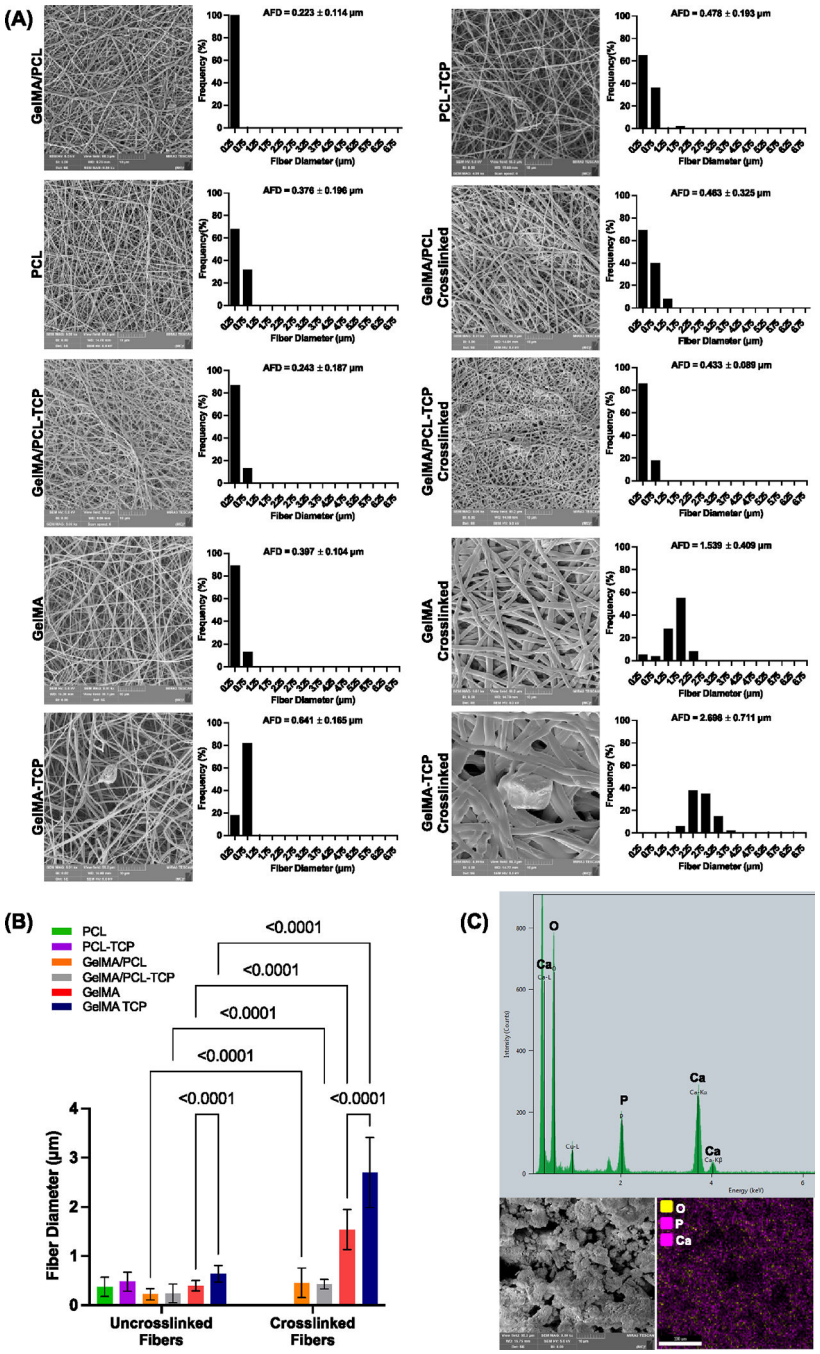

Figure 1.

Morphological and chemical characterizations of manufactured membranes and as-received beta-tricalcium phosphate (TCP). (A) Representative SEM images and histograms showing the fiber diameter frequency and average fiber diameter (AFD) with standard deviation for the manufactured scaffolds before and after crosslinking ($n = 3$). (B) Bar graph comparing the fiber diameter between groups. Data shown as mean ± SD. (C) Energy-dispersive X-ray spectroscopy (EDS) results confirm the presence of Ca, P, and O with an average Ca/P ratio of 1.7, with representative SEM images for TCP ($n = 3$).

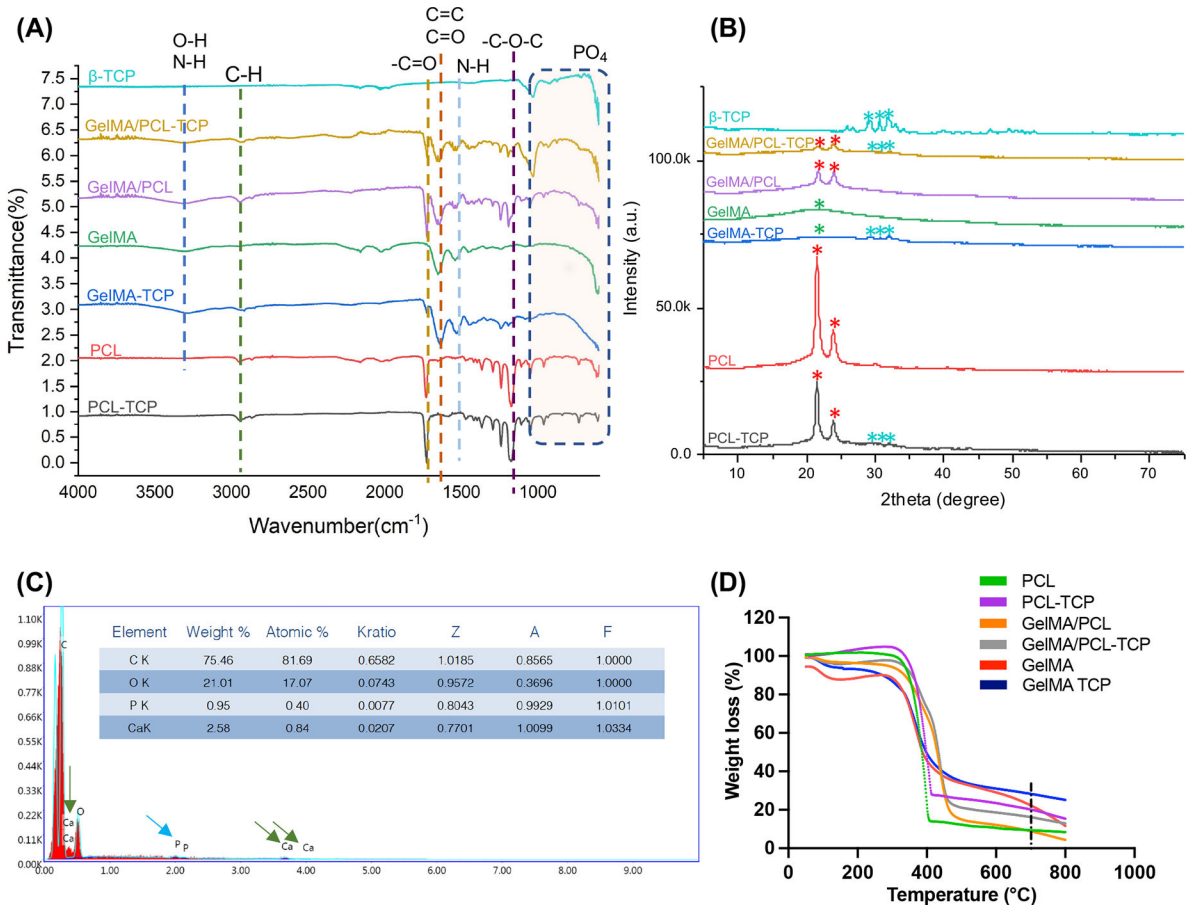

Figure 2.

Physicochemical characterizations of assembled membranes. (A) Fourier-transform infrared spectroscopy (FTIR) analysis of the scaffolds ($n = 3$). (B) X-ray diffraction (XRD) analysis of the scaffolds—red asterisk showing characteristic peaks for PCL; green ones for GelMA; clear blue ones for TCP ($n = 3$). (C) Energy-dispersive X-ray spectroscopy (EDS) analysis of a GelMA/PCL membrane containing 15 wt % of TCP confirms the successful compound incorporation within the fibers. Blue arrows indicate phosphate peaks and green arrows indicate calcium peaks ($n = 3$) (D) Weight loss of polymers measured by thermogravimetric analysis (TGA); black dashed line marking the 700 °C, a standard temperature used to measure the residual weight ($n = 3$).

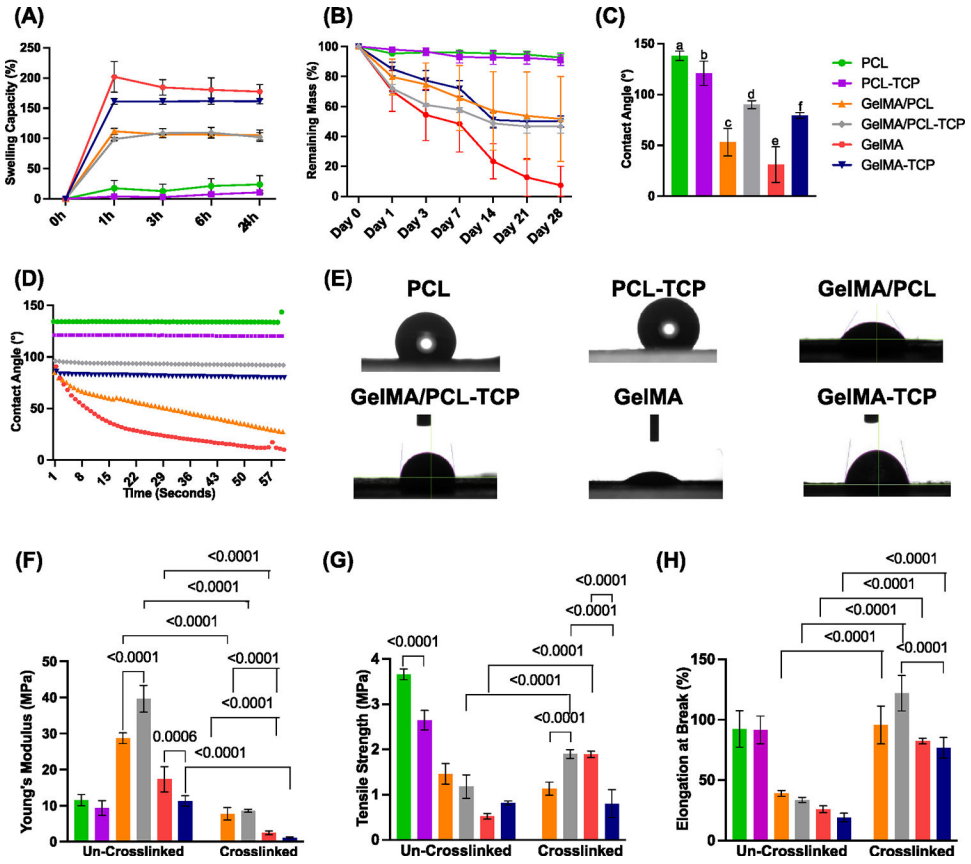

Figure 3.

Swelling, degradation, contact angle, and mechanical characterizations of assembled membranes. (A) The swelling capacity of all membranes at different time points for 24 h ($n = 3$). Note a higher swelling for GelMA pure and TCP-incorporated membranes. (B) Degradation profile of all membranes at several time points ($n = 3$). Note an almost complete degradation for pure GelMA membranes after 28 days. (C) Averaged contact angle measurements ($n = 3$); different lowercase letters denote statistical differences between groups. (D) Individual contact angle data over time points ($n = 3$). (E) Representative contact angle images between water and the assembled membranes ($n = 3$). (F) Young's modulus (MPa, $n = 4$). (G) Tensile strength (MPa, $n = 4$). (H) Elongation at break (%, $n = 4$) under dry (uncrosslinked) and wet (crosslinked) conditions.

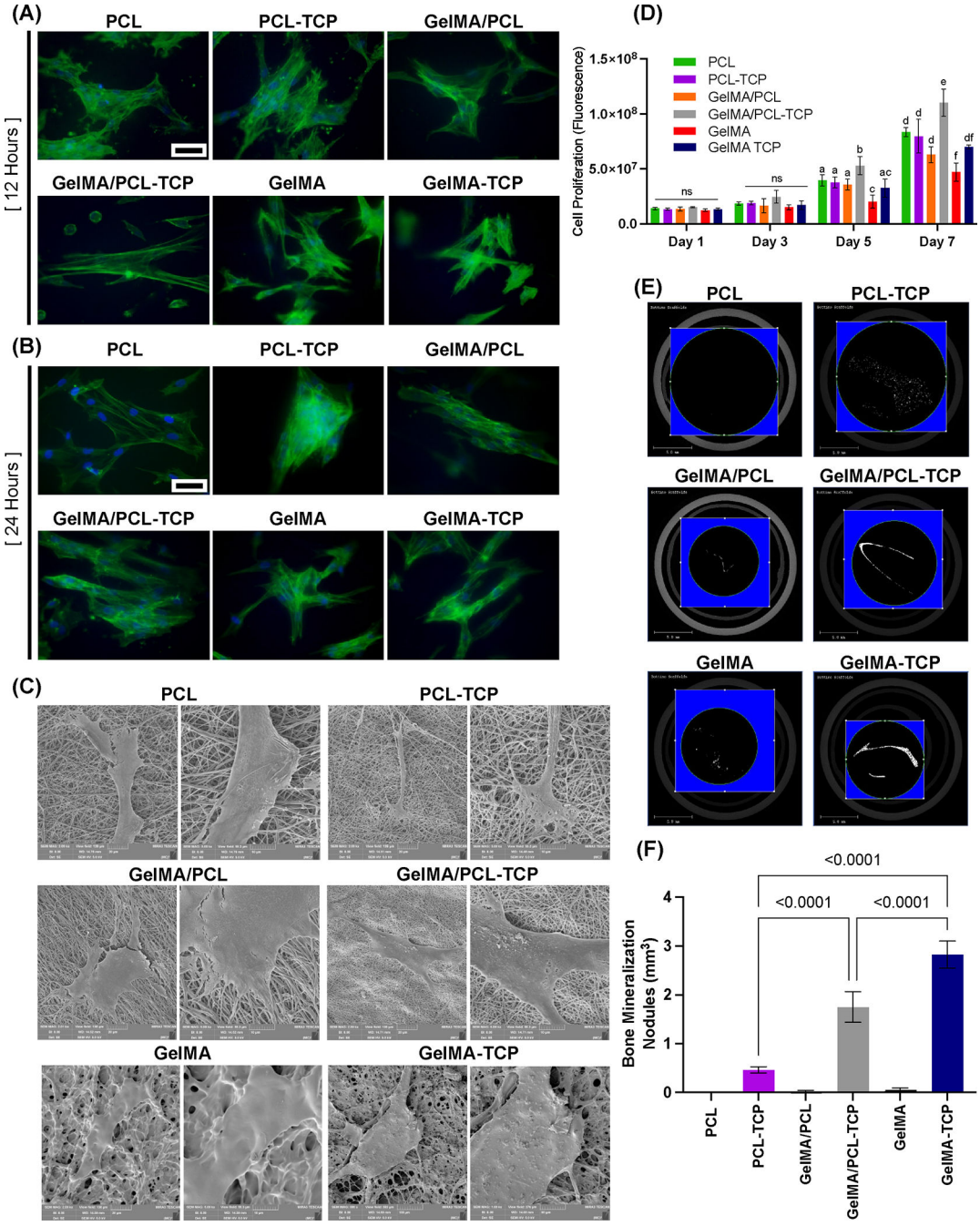

Figure 4.

Immunofluorescent staining of F-actin in aBMSCs seeding on membranes, indicating cell attachment after 12 h (A) and 24 h (B)—scale bar: 50 μm (n = 3). (C) Representative SEM images showing cell–membrane interaction after a 7-day seeding on the membranes (n = 3). (D) alarmarBlue Cell Proliferation results of 1, 3, 5, and 7 days indicate that GelMA/PCL-TCP promoted cell proliferation significantly higher than others (n = 4)—different lowercase letters denote statistical differences between groups. (E) Representative images of Micro-CT

showing the in vitro bone mineralization nodules formation ($n = 3$). (F) Quantified bone volume analysis of aBMSCs after 21 days of osteogenic induction ($n = 3$).

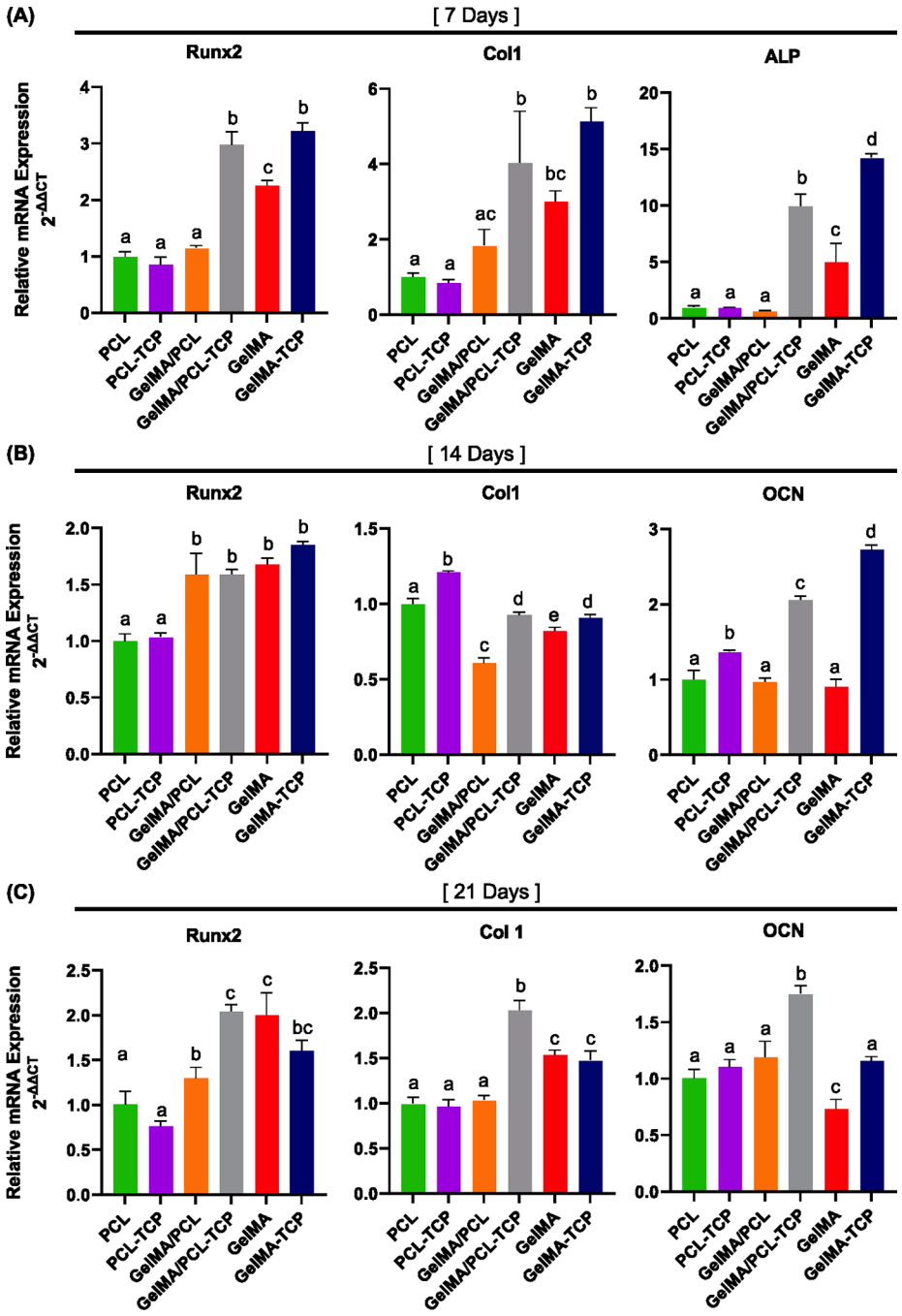

Figure 5.

Osteogenic marker expression after 7 days (A), 14 days (B), and 21 days (C) were evaluated by RT-PCR. Runt-related transcription factor 2 (RUNX2), collagen type 1 (Col1), alkaline phosphatase (ALP), and osteocalcin (OCN) ($n = 3$). Different lowercase letters denote statistical differences between groups.

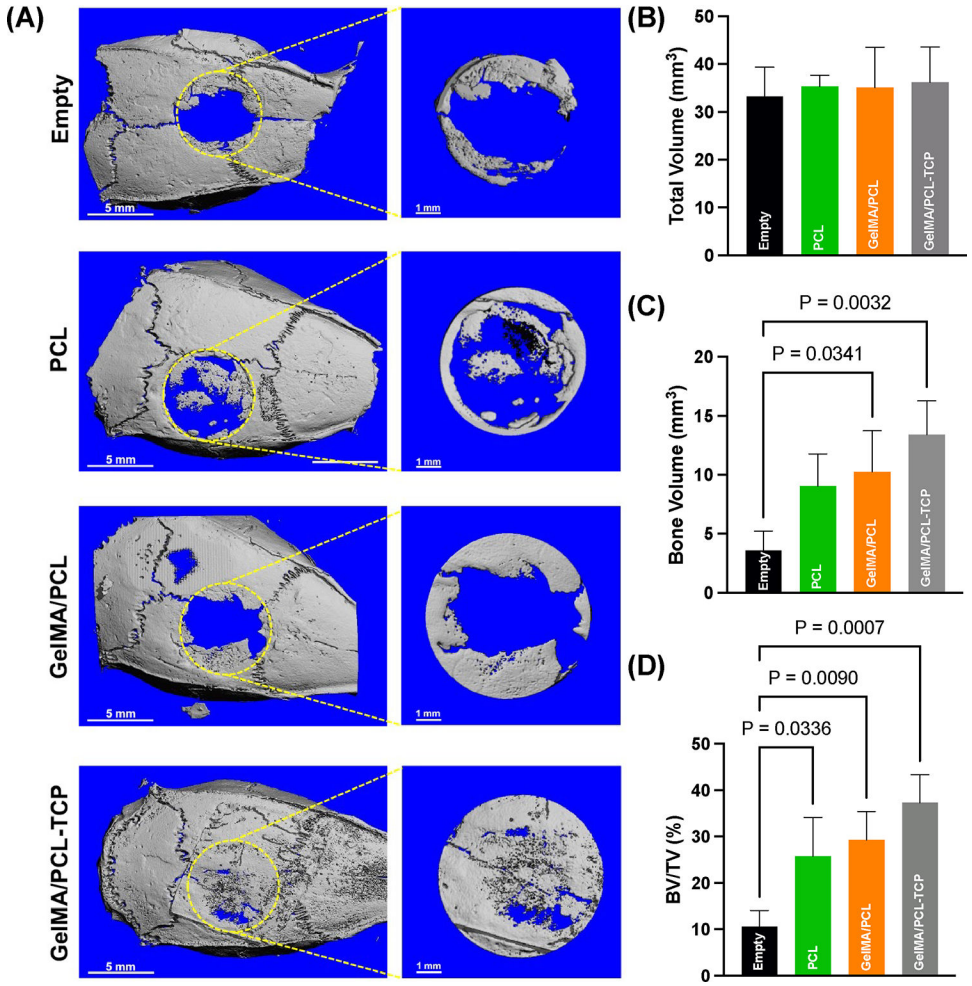

Figure 6.

(A) Micro-computed tomography (μCT) of the bone defects with or without (empty) scaffolds after 6 weeks post-implantation (n = 6). Yellow dashed lines highlight the areas assessed for bone quantification. Scale bar: 5 and 1 mm. (B) Quantitative total volume of the defect, no significant differences between groups. (C) Newly regenerated bone volume present inside the defect; note a significantly higher amount of bone formed evoked by the GelMA/PCL-TCP group followed by GelMA/PCL compared to the empty defect. (D) Ratio between bone volume and total volume defect led by different treatments; it is possible to see an increase in BV/TV for the three employed membranes compared to empty defects, with a higher ratio for GelMA/PCL-TCP.

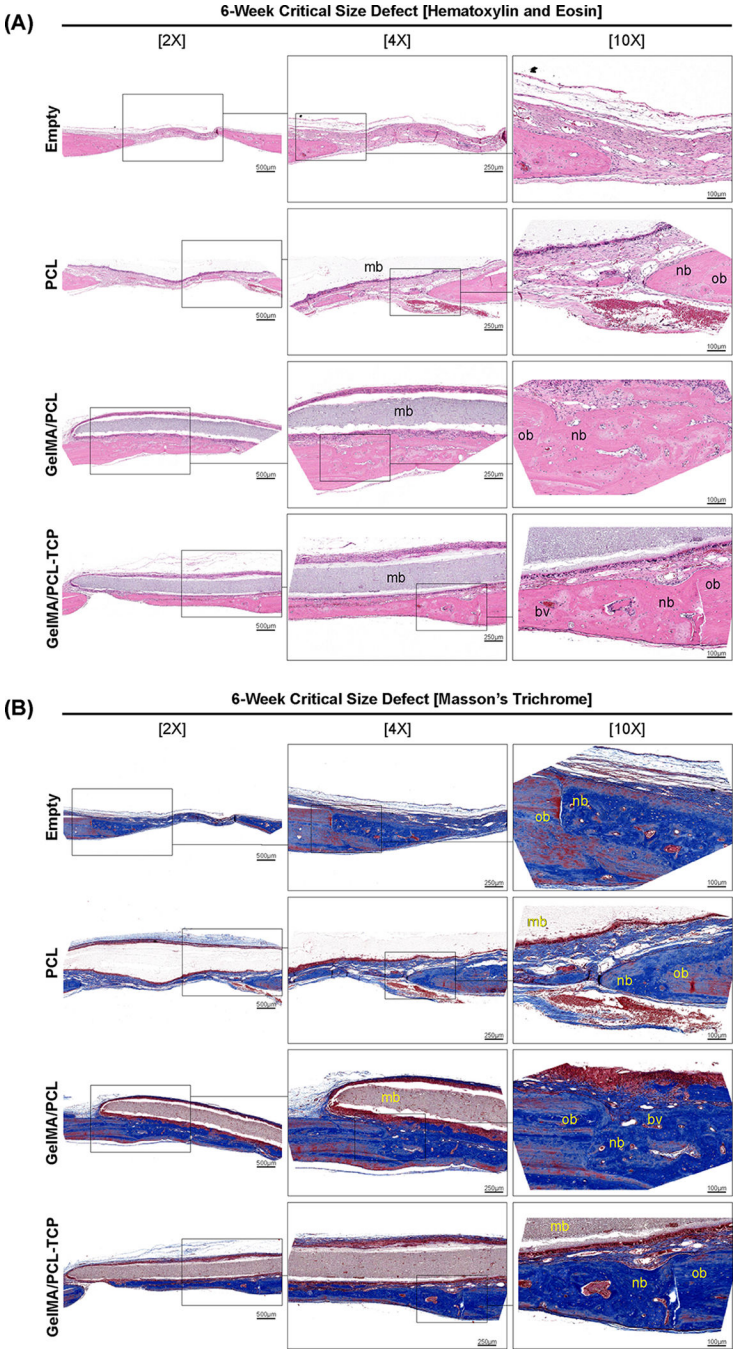

Figure 7.

(A) Hematoxylin and eosin and (B) Masson's trichrome-stained slices of rat calvaria critical-size defects after 6 weeks. Bone formation was observed in all groups, with a significant amount of mature bone in the GelMA/PCL-TCP scaffold group. The defect area in the empty and PCL groups was filled with a small amount of bone and more fibrous connective tissue. New bone is indicated with (nb), original bone (ob), blood vessel (bv), and membrane remnants over the defect (mb). Three consecutive magnifications 2×, 4×, and 10×, with 500, 250, and 100 μm scale bars, respectively.

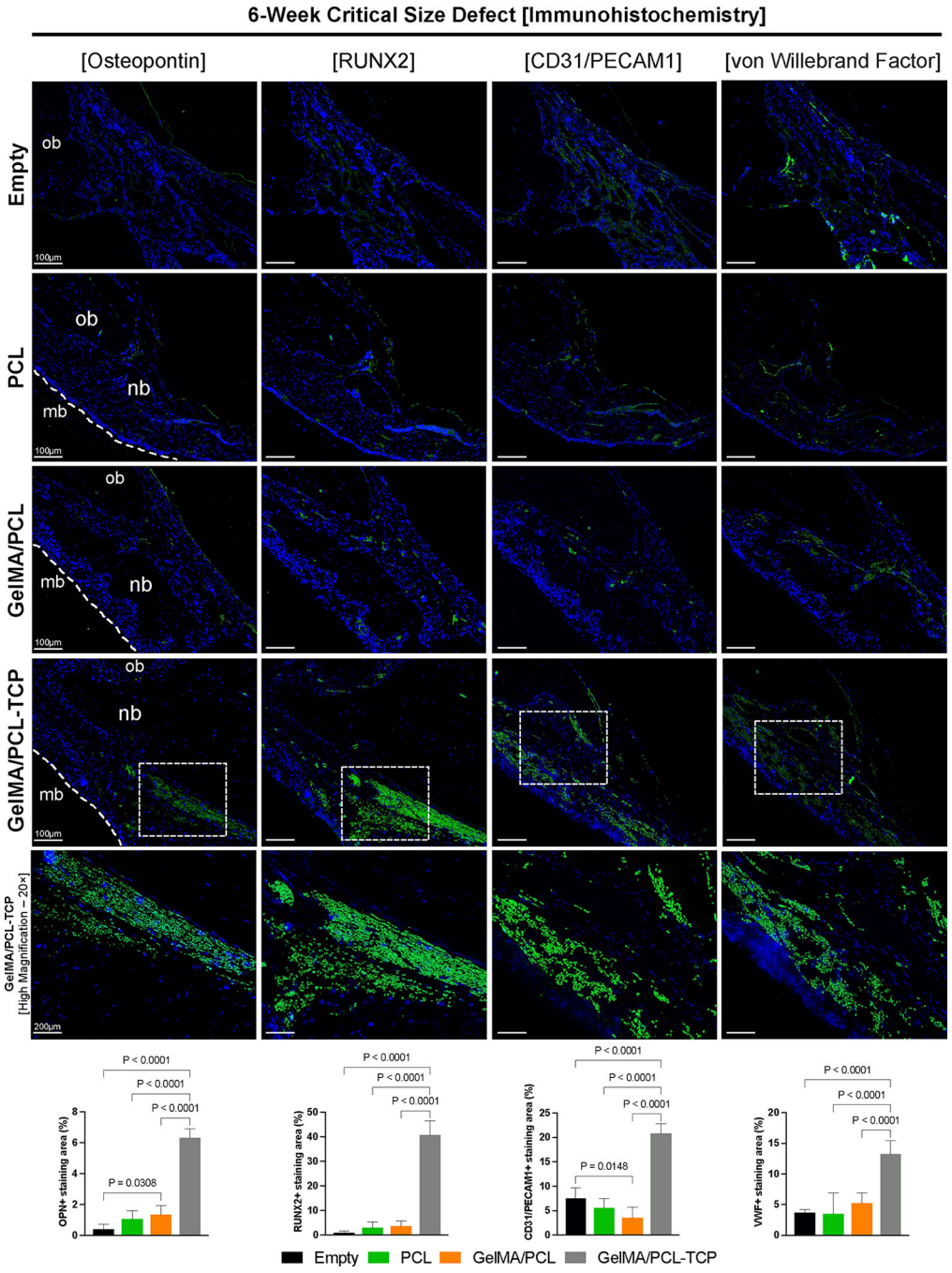

Figure 8.

In vivo 6-week rat critical-size defect immunohistochemistry evaluation of bone formation (osteopontin and Runt-related transcription factor 2RUNX2) and angiogenesis (cluster of differentiation 31C—D31 or platelet and endothelial cell adhesion molecule 1—PECAM1 and von Willebrand Factor). For the osteogenic markers, higher immunolabeling is seen for the GelMA/PCL-TCP group, compared to the other three. Even for the empty defect, it is possible to see adequate immunoexpression for angiogenesis-wise markers, similar to the PCL and GelMA/PCL groups; however, undoubtedly, higher immunolabeling can be

visualized in the GelMA/PCL-TCP group. Cell nuclei were labeled with DAPI (blue), and antibody binding was visualized using Alexa Fluor 488 (green) secondary antibody. mb: membrane; ob: original bone; nb: new bone. Scale bars: 100 μm and 200 μm for GelMA/PCL-TCP [high magnification]. ImageJ software was utilized to quantify the positively stained area of the four immunomarkers, and they were analyzed by an ordinary one-way ANOVA with Tukey's multiple comparison test. Bar graphs that exhibited the mean values and their corresponding standard deviations were used to present the results.

Table 1.

Optimal Parameters Used to Produce All Membranes Synthesized in the Study

	electrospinning parameters			
	voltage (kV)	**distance (cm)**	**flow rate (mL/h)**	**needle gauge**
PCL	18	18	2	27
PCL-TCP	22	15	1.8	23
GelMA/PCL	18	18	2	27
GelMA/PCL-TCP	20	18	2	23
GelMA	18	15	2	27
GelMA-TCP	20	18	2	23